Computational Studies of Transients in Packed Tubular Chemical Reactors

J. E. CRIDER and A. S. FOSS

University of California, Berkeley, California

Concentration and temperature transients in a packed-bed tubular chemical reactor were calculated from mathematical models in order to determine the effects upon the reactor dynamics of several phenomena. The phenomena studied are the thermal capacity of the packing, the resistance to heat flow between the packing and the fluid, the coupling of temperature and concentration through the rate of chemical reaction, axial fluid mixing, radial fluid mixing, and the loss of heat at the wall. Three mathematical models were used: a two-dimensional finite-stage model, a one-dimensional finite-stage model, and a one-dimensional first-order differential model. The chemical reaction considered in these models was an exothermic, homogeneous, liquid phase, second-order reaction.

Machine calculations of transients following step changes in feed temperature or concentration showed that only the first three phenomena were important. It was also found that concentration transients in some cases initially moved in the direction leading away from the final steady state or overshot the final steady state. Further, a concentration node point was found to exist in the reactor under some circumstances. The one-dimensional models considered were shown to be simple but quantitatively and conceptually useful.

As concentration and temperature disturbances pass through a packed tubular chemical reactor, they are affected by several physical and chemical phenomena. The thermal capacity of the packing slows the passage of temperature disturbances through the reactor; the thermal resistance between the fluid and the packing disperses temperature disturbances; temperature and concentration disturbances interact through the chemical reaction and heat generation rates; axial fluid mixing disperses both temperature and concentration disturbances; and loss of heat at the wall and incomplete radial fluid mixing produce radial gradients in temperature and concentration. The effects of many of these phenomena on the behavior of reactors in transient operation are not well established and may have an importance substantially different from their importance at steady state. For example, the thermal capacity of the packing and the thermal resistance between the packing and the fluid are of major importance dynamically but have no effect on the steady state of a packed reactor with a homogeneous reaction. The purpose of this study is to determine the effects and relative importance of these phenomena from numerical computations of the dynamic behavior of three different mathematical models of a chemical reactor. Knowledge of these phenomena and their importance is essential to the development of a simple reactor model useful in reactor control studies.

The three reactor models used in this study are: a two-dimensional finite-stage model, a one-dimensional finite-stage model, and a first-order partial differential model. While this paper reports no experimental work, the experimental studies by Sinai (*12*) in this laboratory and by Tinkler and Lamb (*14*) have shown that the partial differential model represents well the dynamic behavior of homogeneous reactors. Because of the many similarities of the dynamics of the partial differential model with those of the finite-stage models, it is evident that finite-stage models also provide good representations of packed reactors.

The two-dimensional finite-stage model was proposed by Deans and Lapidus (*4* to *6*). This model is an axially symmetric array of stages. The arrangement of stages in this model and the physical model upon which it is based are shown in Figure 1 of reference 2. Each stage in this model is a continuous stirred-tank reactor and represents physically a void space which is bounded by a group of contiguous particles and in which turbulent fluid mixing occurs. Each stage is fed by the two adjacent stages at the preceding axial position, or row; and each stage feeds the two adjacent stages at the following row. There is no flow of heat or fluid between two stages at the same axial position. Heat does flow, however, between the fluid and the packing within a stage. McGuire and Lapidus (*11*) have recently employed this model to study the transient behavior of a packed catalytic reactor. In the present study, however, the packing is not catalytically active and the reaction occurs in the fluid phase.

The one-dimensional finite-stage model is the one-dimensional analog of the two-dimensional finite-stage model. This model is a simple array of continuous stirred-tank reactors in series. Geometrically, each stage is a cylinder of length d_p and a diameter equal to the reactor diameter. The only difference between this model and the two-dimensional finite-stage model is that this model includes complete radial fluid mixing and thus does not allow for radial gradients of concentration or temperature. Therefore a comparison of the behavior of these two models shows the effects of radial gradients resulting from incomplete radial mixing.

The first-order partial differential model is called here the plug flow model. This model is the simplest of the partial differential models; it does not include radial gradients or axial fluid mixing. The major difference between this model and the one-dimensional finite-stage model is that the mixing stage nature of the finite-stage model simulates axial fluid mixing; thus a comparison of the behavior of the two models shows the effect of this phenomenon.

The parameters used in the mathematical models studied here are those of the packed tubular reactor studied experimentally by Sinai (*12*). The packing of the reactor is inert, nonporous glass beads. In the mathematical representations of the reactor, which is axially symmetric, it is assumed that the fluid velocity, the poros-

ity of the packing, the heat capacity and density of the fluid and of the packing particles, and other parameters are constant; that is, independent of time, axial and radial position in the reactor, species concentrations, and temperature. Although many different studies show that the fluid velocity and the packing porosity are not uniform radially, the accuracy of the dynamic models which result from these assumptions of uniformity has been shown by the experimental work of Sinai (*12*) and of Tinkler and Lamb (*14*) for liquid reactants, which is the case treated here.

The chemical reaction in this reactor is the exothermic homogeneous reaction of sodium thiosulfate and hydrogen peroxide in aqueous solution

$$Na_2S_2O_3 + 2H_2O_2 \rightarrow \text{products} \qquad (1)$$

Spencer (*13*) measured the kinetic parameters and determined that the rate of this reaction, that is, the rate of disappearance of sodium thiosulfate, is

$$R^* = k^* c_A^* c_B^* \exp [E/R_g T^*] \qquad (2)$$

The dimensionless form of this rate is

$$R = 2kc_A (c_A - \delta) \exp [AT/(T_o + T)] \qquad (3)$$

where

$$\delta = c_A - c_B/2 \qquad (3a)$$

It is seen that δ may be used to advantage instead of c_B. Unlike c_B, δ is unaffected by temperature.

The disturbances to which the reactor models are subjected are a step change in either reactant concentration in the feed stream or fluid temperature in the feed stream. Preceding these step changes, the reactors are at steady state. With a digital computer, the differential equations expressing heat and mass balances for the different models are solved. These solutions give the behavior of reactant concentrations, fluid temperature, and packing temperature at various points in the reactor. The effects of the various phenomena are determined by the variation of relevant parameters or by the comparison of behavior of different models in which the phenomena are treated differently.

HEAT AND MASS BALANCE EQUATIONS FOR THE REACTOR MODELS

The Two-Dimensional Finite-Stage Reactor

The heat and component mass balance equations of the two-dimensional finite-stage model have been derived, with slightly different notation, by Deans and Lapidus (*4* to *6*). The dimensionless forms of these equations, including a heat balance equation in the packing, are summarized here.

Each stage of the two-dimensional finite-stage model is identified by an axial position i and a radial position j. The axial position i represents the distance of the stage (i, j) from the entrance of the reactor in terms of d_p; the radial position j represents the outer diameter of the stage in terms of d_p. The exception is the half-stage at the wall $(i, M+1)$, which has an inner diameter of $(M-1)d_p$ and an outer diameter of Md_p. It should be noted that i and j are either both even or both odd for any stage in the model.

A component mass balance on a whole stage (i, j) yields

$$\frac{dc_{A_{i,j}}}{dt} = \left(\frac{2j-3}{4j-4}\right) c_{A_{i-1,j-1}} + \left(\frac{2j-1}{4j-4}\right) c_{A_{i-1,j+1}} - c_{A_{i,j}} - R_{i,j} \qquad (4)$$

A mass balance on a half stage at the axis $(i, 1)$, which occurs only on odd axial positions, or rows (that is, where i is odd), gives

$$\frac{dc_{A_{i,1}}}{dt} = c_{A_{i-1,2}} - c_{A_{i,1}} - R_{i,1} \qquad (5)$$

A mass balance on the half stage at the wall $(i, M+1)$, which occurs only on alternate rows (odd rows if $M+1$ is odd, even rows if $M+1$ is even), is

$$\frac{dc_{A_{i,M+1}}}{dt} = c_{A_{i-1,M}} - c_{A_{i,M+1}} - R_{i,M+1} \qquad (6)$$

Heat transport between stages is by convection only. A heat balance on the fluid in a whole stage (i, j) that is not a wall stage yields

$$\frac{dT_{i,j}}{dt} = \left(\frac{2j-3}{4j-4}\right) T_{i-1,j-1} + \left(\frac{2j-1}{4j-4}\right) T_{i-1,j+1} - T_{i,j} + R_{i,j} + Hp\,(T_{p_{i,j}} - T_{i,j}) \qquad (7)$$

A heat balance on the fluid in a half stage at the axis $(i, 1)$ yields

$$\frac{dT_{i,1}}{dt} = T_{i-1,2} - T_{i,1} + R_{i,1} + Hp\,(T_{p_{i,1}} - T_{i,1}) \qquad (8)$$

At the wall stages, the flow of heat through the wall is proportional to the difference between the wall temperature and the temperature of the fluid in the wall stage. A heat balance on the fluid in a whole stage at the wall (i, M), which occurs on alternate rows (odd rows if M is odd, and even rows if M is even), yields

$$\frac{dT_{i,M}}{dt} = \left(\frac{2M-3}{4M-4}\right) T_{i-1,M-1} + \left(\frac{2M-1}{4M-4}\right) T_{i-1,M+1} - T_{i,M} + R_{i,M} + Hp\,(T_{p_{i,M}} - T_{i,M}) + \left(\frac{4M}{4M-4}\right) Hw_2\,(T_w - T_{i,M}) \qquad (9)$$

A heat balance on the fluid in a half stage at the wall $(i, M+1)$ yields

$$\frac{dT_{i,M+1}}{dt} = T_{i-1,M} - T_{i,M+1} + R_{i,M+1} + Hp\,(T_{p_{i,M+1}} - T_{i,M+1}) + \left(\frac{4M}{2M-1}\right) Hw_2 (T_w - T_{i,M+1}) \qquad (10)$$

The terms $4M/(4M-4)$ and $4M/(2M-1)$ in the last two equations represent the ratio of the wall area of the stage to the area of the stage normal to the fluid flow.

A heat balance on the solid in any stage (i, j) yields

$$\frac{dT_{p_{i,j}}}{dt} = \frac{Hp}{\beta - 1} (T_{i,j} - T_{p_{i,j}}) \qquad (11)$$

A mass balance on the second reactant yields equations similar to Equations (4), (5), and (6). These equations may be appropriately subtracted from the corresponding equations for the first reactant to give differential equations describing the $\delta_{i,j}$, the variable δ at stage (i, j). These differential equations show that $\delta_{i,j}$ is independent of temperature; therefore, if there is no radial difference in δ in the feed stream, then there is no radial difference in δ in the bed, and thus δ is independent of j. The resulting equation for δ at row i is

$$\frac{d\delta_i}{dt} = \delta_{i-1} - \delta_i \qquad (12)$$

If there is no concentration step in the feed stream, the solution to Equation (12) is

$$\delta_i = \delta_o \tag{13}$$

If there is a concentration step in the feed stream, Equation (12) was integrated numerically, although its integral can be expressed in terms of simple functions.

The reaction term at stage (i, j) in terms of δ is

$$R_{i,j} = 2kc_{A_{i,j}} (c_{A_{i,j}} - \delta_i) \exp [AT_{i,j}/(T_o + T_{i,j})] \tag{14}$$

The above equations comprise a set of simultaneous, first-order, ordinary differential equations which describe the behavior of the concentration, fluid temperature, and solid temperature in the two-dimensional finite-stage model. These equations were integrated here by the Runge-Kutta-Gill method (7).

The initial conditions for these differential equations are the initial steady state solutions; these are the solutions to the nonlinear algebraic equations which result when the derivatives in the above equations are set equal to zero. At steady state, $T_{p_{i,j}}$ is equal to $T_{i,j}$. The remaining algebraic equations were solved with the Newton-Raphson method for simultaneous equations (9).

The One-Dimensional Finite-Stage Model

The heat and component mass balance equations of the one-dimensional finite-stage model may be obtained by simplifying the equations of the two-dimensional model. The equations for the one-dimensional finite-stage model are summarized here in dimensionless form.

Each stage is characterized by an axial position i, which represents the distance of the stage from the entrance of the reactor in terms of d_p. A mass balance on reactant A in stage i gives

$$\frac{dc_{A_i}}{dt} = c_{A_{i-1}} - c_{A_i} - R_i \tag{15}$$

A heat balance on the fluid yields

$$\frac{dT_i}{dt} = T_{i-1} - T_i + R_i + Hp\,(T_{p_i} - T_i) + \frac{4Hw_1}{M}(T_w - T_i) \tag{16}$$

The wall heat transfer coefficient in this model Hw_1 is an effective heat transfer coefficient which must reflect not only the resistance to heat transfer through the wall, but also the resistance to the radial flow of heat through the bed. The relation between Hw_1 and Hw_2, the actual heat transfer coefficient *at the wall*, is presented elsewhere (2). The relationship between these two coefficients is needed to insure that the heat lost through the walls of each model is identical.

A heat balance on the solid yields

$$\frac{dT_{p_i}}{dt} = \frac{Hp}{\beta - 1}(T_i - T_{p_i}) \tag{17}$$

The equation for δ is Equation (12). The reaction term at stage i is

$$R_i = 2kc_{A_i} (c_{A_i} - \delta_i) \exp [AT_i/(T_o + T_i)] \tag{18}$$

As for the previous model, these differential equations were integrated by the Runge-Kutta-Gill method (7) and the steady state equations were solved by the Newton-Raphson method for simultaneous equations (9).

The Plug Flow Model

Because the plug flow model does not include axial or radial dispersion, the heat and component mass balance equations of this model are first-order partial differential equations. In dimensionless form, the mass balance equation for component A is

$$\frac{\partial c_A}{\partial t} + \frac{\partial c_A}{\partial x} = -R \tag{19}$$

The heat balance equation for the fluid is

$$\frac{\partial T}{\partial t} + \frac{\partial T}{\partial x} = R + Hp\,(T_p - T) + \frac{4Hw_p}{M}(T_w - T) \tag{20}$$

Just as is Hw_1, Hw_p is an effective wall heat transfer coefficient. There is a slight difference between Hw_1 and Hw_p, because the finite-stage model is a discrete model and the plug flow model is a discontinuous model. From reference 3 the relationship between these two coefficients is

$$\frac{4Hw_p}{M} = \ln\left(1 + \frac{4Hw_1}{M}\right) \tag{21}$$

Because Hw_1 is usually small, the difference between Hw_p and Hw_1 is usually minor.

A heat balance on the solid yields

$$\frac{\partial T_p}{dt} = \frac{H_p}{\beta - 1}(T - T_p) \tag{22}$$

The equation for δ is

$$\frac{\partial \delta}{\partial t} + \frac{\partial \delta}{\partial x} = 0 \tag{23}$$

If there is no concentration step, the solution to Equation (23) is

$$\delta(t, x) = \delta_o \text{ (constant)} \tag{24}$$

These differential equations are hyperbolic and are easily treated by the method of characteristics (1, 10). The characteristic curves in this case are the lines

$$\left.\begin{aligned} &\text{I:} \quad t - x = z \text{ (a constant)} \\ &\text{II:} \quad x = y \text{ (a constant)} \end{aligned}\right\} \tag{25}$$

These characteristics in the t-x plane are shown in Figure 1. The differential equations become

$$\left(\frac{dc_A}{dt}\right)_I = \left(\frac{dc_A}{dx}\right)_I = -R \tag{26}$$

$$\left(\frac{dT}{dt}\right)_I = \left(\frac{dT}{dx}\right)_I = R + Hp\,(T_p - T) + \frac{4Hw_p}{M}(T_w - T) \tag{27}$$

$$\left(\frac{d\delta}{dt}\right)_I = \left(\frac{d\delta}{dx}\right)_I = 0 \tag{28}$$

$$\left(\frac{dT_p}{dt}\right)_{II} = \frac{Hp}{\beta - 1}(T - T_p) \tag{29}$$

The derivatives in Equations (26), (27), and (28) are convective derivatives, or derivatives following the fluid motion, because the lines I are the lines in the t-x plane along which the fluid travels through the reactor.

Boundary conditions are needed for the solution of these equations. It will be seen that discontinuities travel with the fluid along lines I; and in particular, discontinuities in the feed at time zero travel along the line t-$x = 0$, or $t = x$. For such discontinuities, regions of the reactor for which $x > t$ are still at steady state. Therefore the proper boundary of the unsteady state region in the t-x plane is $t = x$, not $t = 0$.

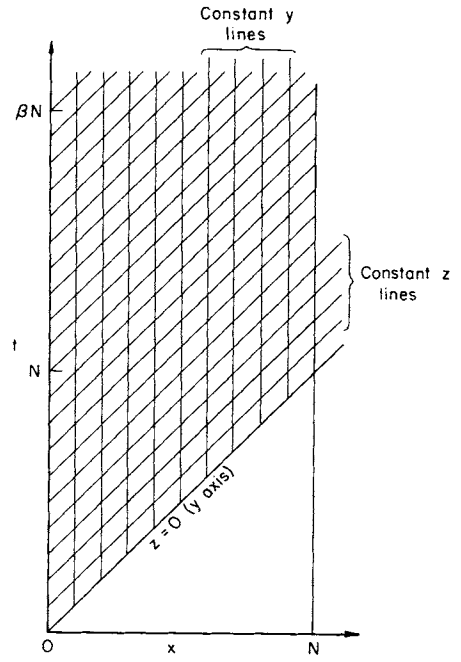

Fig. 1. Characteristic lines in space-time for the plug flow model with finite *Hp*.

At steady state, the fluid temperature and the particle temperature are equal at every point in the reactor, from Equation (22). This same initial steady state profile for particle temperature obtains along the line $t = x$, because, according to Equation (29), the particle temperature profile does not change below this line and the particle temperature is continuous at this line.

The concentration and fluid temperature profiles along the line $t = x$ can be obtained by integrating Equations (26) and (27) along this line, with the final feed concentration and feed temperature as feed conditions and with T_p in Equation (27) equal to the initial steady state temperature, which is a function of x. The concentration and fluid temperature profiles obtained in this manner are not in general identical to the initial steady state profiles, which hold below this line, for $t < x$. The differences between the profiles found in this manner and the initial steady state profiles represent the discontinuities in concentration and fluid temperature which travel with the fluid through the reactor. Further, a feed step either in concentration or in temperautre causes a step both in concentration and in fluid temperature. Integration of Equations (26) through (29) in the unsteady state period, however, shows that these step changes are usually not the largest changes that occur in concentration or fluid temperature in the reactor.

Equations (26) and (27) were numerically integrated on the boundary $t = x$ with the Runge-Kutta-Gill method (*7*). In the unsteady state region, Equations (26), (27), and (29) are integrated with the two-dimensional modified Euler iterative method (*1*). Because Equation (29) is linear, T_p can be expressed as an explicit function of T in the method's difference equations and can therefore be eliminated from the iterations (*8*).

An interesting modification of the plug flow model is made with the assumption that the packing and the fluid are always in thermal equilibrium, in which case *Hp* is infinite and thus there is no thermal resistance between the packing and the fluid. A heat balance on the fluid and the packing in this case gives

$$\beta\frac{\partial T}{\partial t} + \frac{\partial T}{\partial x} = R + \frac{4Hw_p}{M}(T_w - T) \qquad (30)$$

In this case, the characteristic curves for concentration discontinuities are lines *I*, as before, but the characteristic curves along which temperature discontinuities travel are not lines *I*, but the lines

$$III: \qquad \beta x - t = y \text{ (a constant)} \qquad (31)$$

Equation (30) becomes

$$\left(\frac{dT}{dx}\right)_{III} = R + \frac{4Hw_p}{M}(T_w - T) \qquad (32)$$

A temperature discontinuity in the feed at time zero travels along the line $\beta x - t = 0$, or $t = \beta x$; that is, with

Table 1. Numerical Values of Parameters (*12*)

Parameter	Symbol	Value
$Na_2S_2O_3$ feed concentration	c_A^* $(x = 0)$	0.325×10^{-3} or 0.390×10^{-3} moles/cc. (see text)
H_2O_2 feed concentration	c_B^* $(x = 0)$	1.3×10^{-3} moles/cc.
Reference concentration	c_r	0.325×10^{-3} moles/cc.
Feed temperature	T^* $(x = 0)$	27° or 37°C. (see text)
Wall temperature	T_w^*	27° or 37°C. (see text)
Reactor length	L	30 cm.
Reactor diameter	D_T	2.54 cm.
Particle diameter	d_p	0.3 cm.
Void fraction of the bed	ϵ	0.37
Fluid velocity	v	8.36 cm./sec.
Particle residence time	d_p/v	0.0359 sec.
Fluid density	ρ_f	1. g./cc.
Fluid heat capacity	c_f	1. cal./(g.)(°C.)
Particle density	ρ_p	2.23 g./cc.
Particle heat capacity	c_p	0.20 cal./(g.)(°C.)
Particle surface-to-volume ratio	a_p	20. sq. cm./cc.
Particle-fluid heat transfer coefficient	h_p	0.0406 cal./(sec.)(sq. cm.)/°C. [300 B.t.u./(hr.)(sq. ft.)/°F.]
Wall heat transfer coefficient	h_w	0.09201 cal./(sec.)(sq. cm.)/°C. [679 B.t.u./(hr.)(sq. ft.)/°F.]
Energy of activation	E	18.3 kcal./mole $Na_2S_2O_3$
Pre-exponential coefficient	k^*	0.685×10^{15} cc./(sec.)(mole $Na_2S_2O_3$)
Heat of reaction	$(-\Delta H)$	132 kcal./mole $Na_2S_2O_3$
Adiabatic temperature rise	ΔT_a	42.9 °C.

TABLE 2. NUMERICAL VALUES OF DIMENSIONLESS PARAMETERS

Parameter	Symbol	Value
Reactor length	N	100
Reactor diameter	M	8.47 (rounded to integer: 8)
Heat capacity parameter	β	1.7594
Particle-fluid heat transfer coefficient	Hp	0.04983
Wall heat transfer coefficient	Hw_2	0.01101
Overall heat transfer coefficients	Hw_1	0.01038
	Hw_p	0.01035
Activation energy*	A	30.69
Pre-exponential coefficient*	k	3.746×10^{-4}
Reference temperature/adiabatic temperature rise*	T_o	6.997

* The values of A, k, and T_o are based upon a reference temperature of 27°C.

a velocity which is $1/\beta$ times the fluid velocity. It can be shown that, for a step change in feed concentration or feed temperature, the reactor is at a final steady state for $t > \beta x$. In this case, therefore, the unsteady state region is bounded by the lines $t = x$ and $t = \beta x$.

Description of the Computations

A Fortran IV computer program was written for the numerical integration of each of the three models considered here: the two-dimensional finite-stage model, the one-dimensional finite-stage model, and the plug flow model with finite Hp. The input to the programs is the operating and reactor parameters, which can be chosen to represent a variety of reactors, such as adiabatic reactors, non-adiabatic reactors, isothermal reactors, packed-bed heat exchangers without chemical reactions, etc. The output of the programs can include machine-plotted graphs of concentration and temperature axial profiles at selected values of time and the time-dependent behavior of concentration and fluid temperature at selected axial positions.

For a reactor with a length of one hundred particle diameters and unsteady state behavior lasting 2.6 reactor residence times, the computing time on the IBM 7094 for the plug flow model with space and time increments each of one dimensionless unit was 0.9 min. and for the one-dimensional finite-stage model with time increments of one dimensionless unit the computing time was 2.0 min. For the same reactor, with a diameter of eight particle diameters, the program for the two-dimensional stage model required less than 10 min. The additional time required for the preparation of a plot tape varied, depending upon the model and the form of the graphs. The actual plotting was done off-line with the plotting tape, and required 15 min. on the IBM 1401 for the production of four graphs including a total of seventy curves or about 7,500 calculated points.

Table 1 shows the numerical values of the parameters used in these machine calculations; these values are typical of Sinai's (*12*) experimental reactor. The values of the corresponding dimensionless parameters are shown in Table 2.

Machine calculations were made both for a step increase in the concentration of sodium thiosulfate in the feed and for a step in the temperature of the feed. In all calculations, the concentration of hydrogen peroxide in the feed was the same. For the calculations in which there was a step in feed concentration, the feed concentration of sodium thiosulfate was increased by 20% from 0.325 moles/liter to 0.390 moles/liter, while the feed temperature and the wall temperature remained constant at 37°C. In the other calculations, the feed concentration of sodium thiosulfate remained constant at 0.325 moles/liter and the wall temperature remained constant at 27°C., while the temperature of the feed was increased from 27° to 37°C.

Some of the parameters of the models had values different from those given in Tables 1 and 2 for those machine calculations in which the effects of certain phenomena, which these parameters represent, were studied. Thus, in calculations for the nonadiabatic reactor, Hw_1 and Hw_p had the values given in Table 2; for the adiabatic reactor, these heat transfer coefficients were zero. Also, in most calculations, Hp had the value given in Table 2, while in the others, Hp was infinite and the fluid temperature and the particle temperature were identical.

RESULTS

The response of the adiabatic reactor to a 20% step increase in reactant concentration is shown in Figures 2 and 3, which show the concentration and fluid temperature at selected axial positions as functions of dimensionless time.

This response, determined through the one-dimensional finite-stage model, illustrates the effects of all the phenomena which dominate the dynamics. It is seen from Figure 2 that the initial part of the concentration disturbance, although somewhat dispersed, passes through the reactor at the fluid velocity, which is unity in the dimensionless variables used here. Figure 3 shows that this initial concentration disturbance, as it passes through the reactor, causes a temperature disturbance; this effect

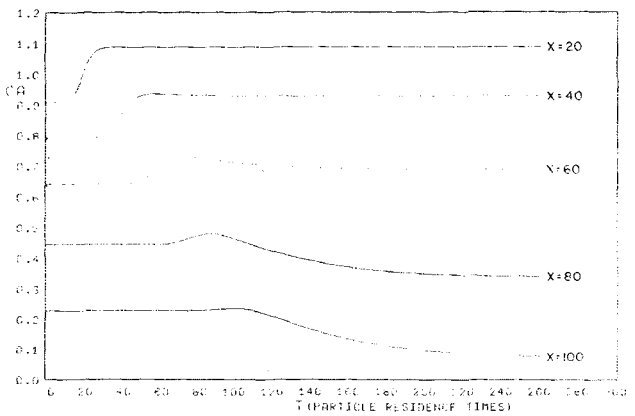

Fig. 2. Response of concentration at selected axial positions to a concentration step. One-dimensional finite-stage model, adiabatic, *Hp* finite.

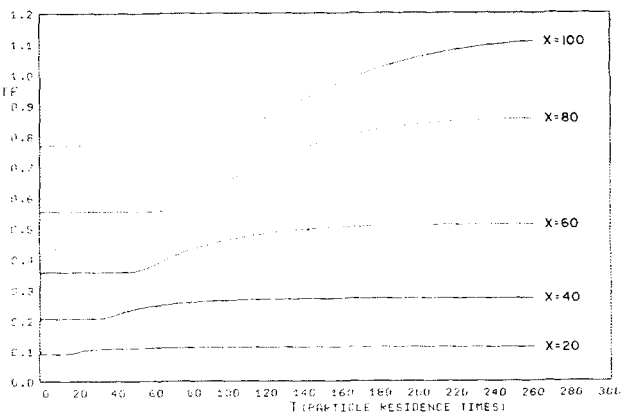

Fig. 3. Response of temperature at selected axial positions to a concentration step. One-dimensional finite-stage model, adiabatic, *Hp* finite.

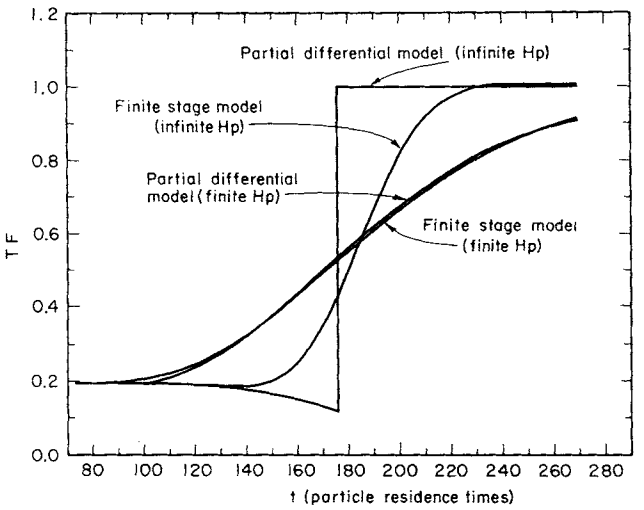

Fig. 4. Response of temperature at exit ($x = 100$) to a temperature step in the plug flow model with infinite *Hp*. Comparison with plug flow model with finite *Hp* and one-dimensional finite-stage with infinite and finite *Hu*. Adiabatic.

results from the coupling of heat and mass in the reaction. The dispersion of these initial concentration and temperature disturbances is caused by axial fluid mixing. Concentration and temperature in the reactor continue to change, approaching steady states that are consistent with the new feed conditions. Because of the thermal capacity of the packing, the major part of the temperature change travels through the reactor at $1/\beta$ (here, 1/1.76) times the fluid velocity; this temperature change is quite dispersed because of the resistance of heat flow between the packing and the fluid. The temperature change continues to effect a change in concentration, which in turn modifies the temperature change, through the reaction coupling.

The effects outlined above were determined either by comparison of the responses of two different models operating under identical conditions or by comparison of responses of one model for different values of the parameters. For these comparisons, computer calculations were made of the dynamic behavior of concentration and temperature in the reactor for fourteen different combinations of the reactor model, the feed disturbance (temperature step or concentration step), and values of various parameters. The detailed results of these calculations are contained in reference 3. Only a representative sample of the results is presented here.

The Effects of the Thermal Capacity of the Packing and of the Reaction Coupling

The thermal capacity of the packing slows the velocity of the temperature disturbance. This effect is most clearly seen in the response to a temperature step of the plug flow model for the case of infinite *Hp*. This response is shown in Figure 4 for a step in feed temperature from 27° to 37°C. Also shown in Figure 4 are the responses to the same step of the one-dimensional finite-stage model with infinite *Hp*, the plug flow model with the value of *Hp* given in Table 2, and the one-dimensional finite-stage model with the same value of *Hp*. All responses shown in this figure are of fluid temperature at $x = 100$. For reference, the response of concentration and temperature in the one-dimensional finite-stage model (with finite *Hp*) for this same step in feed temperature are shown in Figures 5 and 6. The curve labelled $x = 100$ in Figure 6 is identical to the curve labeled *Finite stage model* (*finite Hp*) in Figure 4.

The curve labelled *Partial differential model* (*infinite Hp*) shows most clearly the effect of the heat capacity of the packing. The temperature discontinuity in this model travels along the trajectory $\beta x = t$, a characteristic line *III* [Equation (31)]. The velocity of this discontinuity is $1/\beta$ times the fluid velocity, where β represents the ratio of the total heat capacity in the reactor to the heat capacity of the fluid. The other curves in Figure 4, which show dispersive effects, also indicate that the major change in temperature occurs in the neighborhood of $t = \beta x$.

It may be noted that the response of the plug flow model (partial differential model) with finite *Hp* includes a discontinuity at $t = 100$; but it is too small to be seen in Figure 4. Thus, although this model by nature has concentration and temperature discontinuities along its characteristics, these discontinuities are not necessarily the largest changes in these variables.

The small temperature decrease that precedes the large temperature increase for the two curves in Figure 4 for which *Hp* is infinite is a minor but interesting effect of the reaction coupling. Because of the high temperature behind the slowly moving temperature wave, the reaction here is more complete and the concentration behind the wave is lower than in front of the wave. Because the temperature wave travels slower than the fluid velocity, the fluid carries material of lower concentration into the regions in front of the wave; but the fluid does not also carry heat through the temperature wave because of thermal equilibruim between the particles and the fluid. Thus, in front of the temperature wave, the concentration drops; the rate of reaction, which depends on the

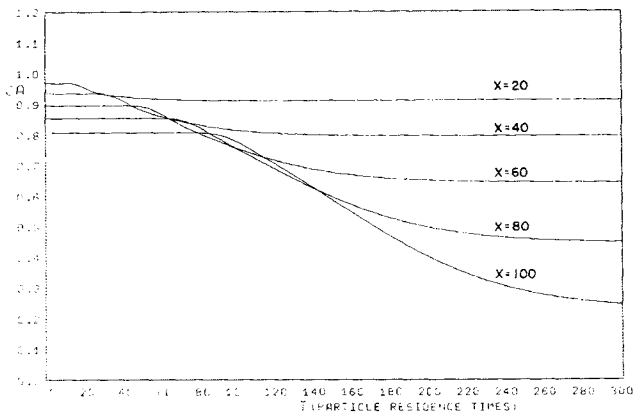

Fig. 5. Response of concentration at selected axial positions to a temperature step. One-dimensional finite-stage model, adiabatic, *Hp* finite.

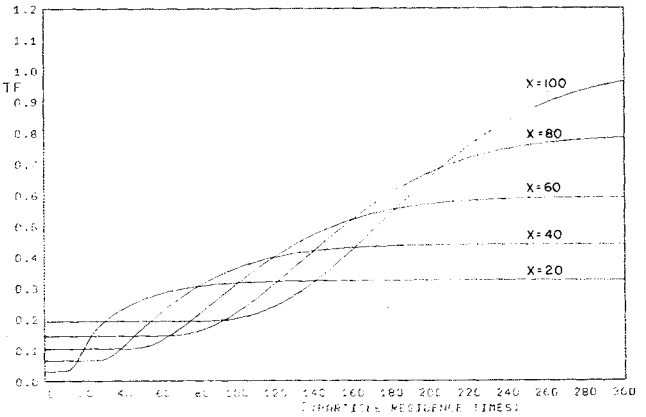

Fig. 6. Response of temperature at selected axial positions to a temperature step. One-dimensional finite-stage model, adiabatic, *Hp* finite.

concentration, drops; and the rate of generation of heat, which is proportional to the rate of reaction, drops. Therefore the temperature drops in the region in front of the temperature wave. For liquid reactors this effect is usually small, however, and it is overshadowed by dispersive effects, as the other curves in Figure 4 show.

Another effect of reaction coupling is the existence in the reactor of a concentration node point with respect to concentration disturbances. This point is the point in the reactor at which the initial and final steady state concentrations are the same; for example, at $x = 67$ for the parameters of Figures 2 and 3. At this point in the reactor, the response of concentration to disturbances in the feed concentration are slight, as interpolation between curves in Figure 2 shows; and the initial and final steady state concentrations at this point are the same. If a reactor to be designed is subject primarily to feed concentration disturbances rather than to feed temperature disturbances, and constancy of conversion is desired, the distance from the inlet to this node point may be an appropriate length for the reactor. It should be noted that this point is determined only from two steady state calculations. However, it should be realized that the fluid temperature at this point varies considerably with disturbances in feed concentration, as Figure 3 shows; further, the concentration at this point varies considerably with disturbances in feed temperature, as Figure 5 shows.

These two effects are but examples of the effects of the coupling of heat and mass through the reaction. Although such effects are apparent in many cases, they were not investigated in detail here. The responses presented here show, however, that the coupling of heat and mass in the reaction and the thermal capacity of the packing have the most important effects on the dynamic behavior of the reactor.

The Effect of Thermal Resistance Between the Fluid and the Packing

The thermal resistance between the fluid and the packing greatly disperses temperature disturbances, and through the reaction coupling it also disperses concentration disturbances. This effect is easily seen from the comparison in Figure 4 of either model with infinite Hp (no thermal resistance) with the same model with a finite value of Hp typical of that measured by Sinai (*12*). Clearly the thermal resistance between the fluid and the packing must be included in any realistic dynamic model of a reactor. And yet, for a homogeneous reaction, this resistance has no effect upon the steady state of the reactor.

In particular, the behavior of the plug flow model with infinite Hp and the plug flow model with finite Hp, as shown in Figure 4, may be compared. In both cases, the major change in temperature occurs at $t = 176$, that is, at $t = \beta x$. The plug flow model with infinite Hp is at steady state after this time. The plug flow model with finite Hp, however, is not at steady state for $t > \beta x$, because of the dispersive effect of the thermal resistance. Because of the severe temperature discontinuities at $t = \beta x$ in the plug flow model with infinite Hp, this model (with Hp infinite) cannot be considered as an accurate model of a tubular reactor. However, this model is conceptually useful because it shows most clearly the effect of the heat capacity of the packing.

The Effect of Axial Mixing

Compared with the dispersion resulting from the thermal resistance between the fluid and the packing, axial mixing resulting from turbulent fluid mixing and molecular diffusion has a very small effect upon the dynamics of the reactor. The plug flow model does not include axial mixing, but the finite-stage models simulate it by the mixing stages. The effects of axial mixing can be obtained then from a comparison of the behavior of these two models.

The behavior of both of these models (with infinite Hp) following a step increase in feed temperature is shown in Figure 4. The behavior of the plug flow model following an increase in feed concentration is shown in Figures 7 and 8. These figures may be compared with Figures 2 and 3 for the finite-stage model. The discontinuities in the plug flow model should appear as vertical lines at $x = t$ rather than as the oblique lines that are actually shown in Figures 7 and 8 and which resulted from a peculiarity of the plotting program.

The major effect of axial mixing is the dispersion of the initial concentration and temperature disturbances that travel with the fluid. These disturbances appear as discontinuities in the plug flow model and as continuous deviations in the finite-stage models. Axial mixing both reduces the magnitude of the deviation of these disturbances from the initial steady state and causes them to begin to appear slightly before one residence time; that is, the downstream part of the disturbance travels slightly faster than the average fluid velocity.

Comparison of these figures reveals that the magnitudes of the discontinuities of the plug flow model provide upper bounds for these initial deviations from steady state in actual reactors. The magnitudes of the discontinuities in the plug flow model are easily determined from the quasi steady state calculation of the concentration and temperature profiles along the line $t = x$ as discussed above.

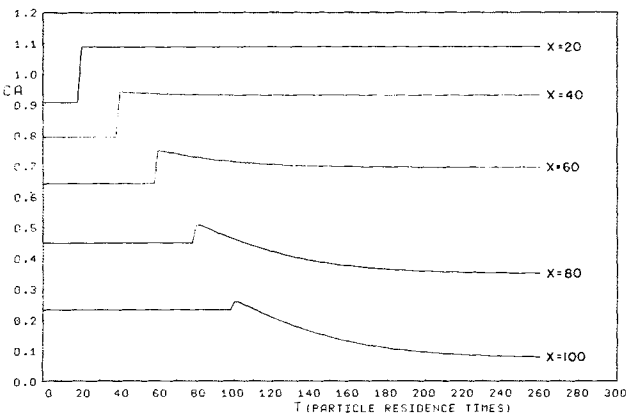

Fig. 7. Response of concentration at selected axial positions to a concentration step. Plug flow model, adiabatic, *Hp* finite.

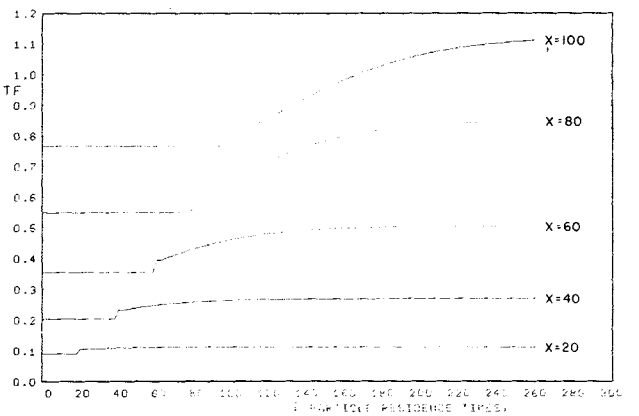

Fig. 8. Response of temperature at selected axial positions to a concentration step. Plug flow model, adiabatic, *Hp* finite.

It may be noted that in some cases the initial concentration disturbance that travels with the fluid is in a direction leading away from the final steady state; in other cases, the initial concentration disturbance overshoots the final steady state value. Such behavior, illustrated in Figure 2, may lead to control difficulties if the effluent concentration is used in feedback control. In all cases, however, concentration and temperature proceed monotonically to their steady state values after this initial disturbance has passed.

It may therefore be concluded that the major dynamic effect of axial mixing, which is the dispersion of the initial concentration and temperature disturbances, is perceptible, but is usually minor.

The Effects of Heat Loss at the Wall and of Radial Gradients

Loss of heat in a reactor reduces the fluid temperature in the reactor, thus reducing the rate of reaction and thus the rate of heat generation, further reducing the fluid temperature. Because the rate of reaction is reduced, the concentrations of the reactants are higher than in the adiabatic reactor. Also, the concentration node point is moved farther from the inlet of the reactor. No specific dynamic effects of heat loss at the wall were seen; that is, all effects seen were those which were predictable from steady state profiles.

The effect of radial gradients was imperceptible. The behavior of the two-dimensional finite-stage model with a disturbance in either feed temperature or feed concentration was almost identical to the behavior of the one-dimensional finite-stage model under the same conditions. This result may be expected because most of the radial resistance to heat flow is at the wall rather than in the bed, as evidenced by the fact that the overall heat transfer coefficient Hw_1 is almost identical to the wall heat transfer coefficient Hw_2. Further, the maximum radial fluid temperature difference is only 6°C. Thus it may be concluded that the effects of radial gradients are very minor for liquid phase reactions unless the reaction rate is extremely sensitive to temperature.

CONCLUSIONS

In summary, the three phenomena which dominate the dynamic behavior of the packed tubular chemical reactor studied here are: thermal capacity of the packing, which causes the major temperature disturbance to travel through the reactor more slowly than the fluid; the coupling of heat and mass in the reaction, through which concentration disturbances and temperature disturbances significantly affect each other; and the resistance to heat transfer between the fluid and the packing, which greatly disperses the major temperature disturbance. Only the second of these, the reaction coupling, affects the steady state of the reactor.

The effects of all three of these phenomena are simulated in both the one-dimensional finite-stage model and the plug flow model. Because both of these models are both accurate and simple, they may be recommended for other studies of the dynamics of a tubular reactor.

The one-dimensional finite-stage model also includes the effects of axial mixing. The major effect of axial mixing is the dispersion of the initial concentration and temperature disturbances that travel with the fluid. This effect is small.

The effects of radial gradients appear to be negligible for liquid phase reactions, and the use of a two-dimensional model which includes these effects appears to be unnecessary.

ACKNOWLEDGMENT

The authors acknowledge with thanks the support of this work by the National Science Foundation, the Computer Center of the University of California, and the Atomic Energy Commission through the Lawrence Radiation Laboratory.

NOTATION

A = dimensionless activation energy, E/R_gT_r
a_p = specific surface area of the packing particles. For spheres, $a_p = 6/d_p$
c_A = dimensionless concentration of reactant A, c_A^*/c_r
CA = representation of c_A on machine-plotted graphs
c_A^* = concentration of reactant A, sodium thiosulfate
c_B = dimensionless concentration of reactant B, c_B^*/c_r
c_B^* = concentration of reactant B, hydrogen peroxide
c_f = heat capacity of the fluid
c_p = heat capacity of the packing particles
c_r = reference concentration, usually a feed concentration
D_T = diameter of the reactor
d_p = average diameter of the packing particles, used here as a fundamental unit of length
E = activation energy of the reaction
Hp = dimensionless heat transfer coefficient between the particles and the fluid, $h_pa_p(1 - \epsilon)d_p/\rho_fc_f\epsilon v$
Hw = dimensionless wall heat transfer coefficient, h_w/ρ_fc_fv
Hw_1 = Hw for the one-dimensional finite-stage model
Hw_2 = Hw for the two-dimensional finite-stage model
Hw_p = Hw for the plug flow model
h_p = heat transfer coefficient between the particles and the fluid
h_w = wall heat transfer coefficient
k = dimensionless kinetic pre-exponential coefficient, $(k^*c_rd_p/v)\exp(-A)$
k^* = kinetic pre-exponential coefficient
L = length of the reactor
M = dimensionless diameter of the reactor, D_T/d_p
N = dimensionless length of the reactor, L/d_p
R = dimensionless rate of reaction, R^*d_p/vc_r
R^* = rate of reaction
R_g = gas constant
T = dimensionless temperature of the fluid, $(T^* - T_r)/\Delta T_a$
TF = representation of T on machine-plotted graphs
T^* = temperature of the fluid
T_o = $T_r/\Delta T_a$, the ratio of the reference temperature to the total adiabatic temperature rise
T_p = dimensionless temperature of the particles, $(T_p^* - T_r)/\Delta T_a$
T_p^* = temperature of the particles
T_r = reference temperature, usually equal to T_w^*
T_w = dimensionless temperature of the wall, $(T_w^* - T_r)/\Delta T_a$
T_w^* = wall temperature
t = dimensionless time, t^*v/d_p
t^* = dimensional time
v = actual average velocity of the fluid through the bed
x = dimensionless axial variable, x^*/d_p
x^* = dimensional distance along the reactor axis
y,z = quantities which are constants along the characteristic curves in space-time for the plug flow model

Greek Letters

β = dimensionless heat capacity parameter, $1 + \rho_pc_p \times (1 - \epsilon)d_p/\rho_fc_f\epsilon$
$(-\Delta H)$ = heat of reaction
ΔT_a = total adiabatic temperature rise for the reaction, $(-\Delta H)c_r/\rho_fc_f$
δ = stoichiometric concentration difference, given in Equation (3a)
δ_o = δ at the inlet of the reactor
ϵ = void fraction of the packed bed

ρ_f = density of the fluid
ρ_p = density of the packing particles

LITERATURE CITED

1. Acrivos, Andreas, *Ind. Eng. Chem.*, **48**, 703 (1956).
2. Crider, J. E., and A. S. Foss, *A.I.Ch.E. J.*, **11**, 1012 (1965).
3. ————, *Univ. California Lawrence Radiation Lab. Rept. No. UCRL-11757* (January, 1965).
4. Deans, H. A., Ph.D. thesis, Princeton University (1960).
5. ———, and Leon Lapidus, *A.I.Ch.E. J.*, **6**, 656 (1960).
6. *Ibid.*, 663.
7. Gill, S., *Proc. Cambridge Phil. Soc.*, **47**, 96 (1951).
8. Gonzales, L. O., and E. H. Spencer, *Chem. Eng. Sci.*, **18**, 753 (1963).
9. Hildebrand, F. B., "Introduction to Numerical Analysis," McGraw-Hill, New York (1956).
10. Jeffrey, Alan, and Tosiya Taniuti, "Non-Linear Wave Propagation," Academic Press, New York (1964).
11. McGuire, M. L., and Leon Lapidus, *A.I.Ch.E. J.*, **11**, 85 (1965).
12. Sinai, José, Ph.D. thesis, Univ. California, Berkeley (1965).
13. Spencer, J. L., Ph.D. thesis, Univ. Pennsylvania, Philadelphia (1961).
14. Tinkler, J. D., and D. E. Lamb, *Chem. Eng. Progr. Symposium Ser. No. 55*, **61**, 155 (1965).

Manuscript received May 17, 1965; revision received December 7, 1965; paper accepted December 10, 1965.

A Correlation of the Frictional Characteristics for Turbulent Flow of Dilute Viscoelastic Non-Newtonian Fluids in Pipes

WARREN A. MEYER

Ling-Temco-Vought, Inc., Dallas, Texas

A formula has been determined which satisfactorily represents, for the existing data, the frictional characteristics of the turbulent flow of a dilute viscoelastic non-Newtonian fluid in a pipe. This formula contains two elastic fluid parameters, one of which is strongly dependent on both polymer solute and concentration and the other appears to be a constant and independent of the polymer solutes which were used in this report. A rheometer is proposed based on this formula which should be useful in classifying fluids of this type.

The purpose of this paper is to propose a formula which, based upon the limited data available, shows promise in predicting the frictional characteristics of turbulent flow of dilute viscoelastic non-Newtonian fluids in pipes. Since no adequate theoretical procedure exists for the evaluation of turbulent boundary-layer flows, the derivation of the above mentioned formula was, by necessity, empirical. Nevertheless, some of the empirical relationships used imply the presence of a basic underlying mechanism, the understanding of which could lead to the formulation of a theoretical procedure.

In the initial work done at this laboratory by Wells (*1*), who used guar gum (J-2P, product of the Western Company) solutions of concentrations from 500 to 4,000 p.p.m. in water, there was a strong implication that the viscoelastic effect of a non-Newtonian fluid on turbulent flow caused a decrease in the Prandtl mixing length constant. A similar conclusion was reached by Elata† and Tirosh in a recent publication (*2*) in which they used very dilute concentrations (50 to 400 p.p.m.) of guar gum ("Jaguar," product of Stein and Hall) in water. The work of Ernst (*3*), however, very conclusively showed that, for a dilute concentration (500 p.p.m.) of CMC 7HSP in water, the mixing length constant in the turbulent portion of the flow was not changed; and there appeared to be a thickening of the laminar and buffer layers of the flow near the wall. In the light of these results, the work of Wells and of Elata and Tirosh were re-evaluated and it was found that, at least for dilute concentrations of viscoelastic fluids, they could be interpreted to show the value of the mixing length constant to be unchanged. It is the evaluation and interpretation of the results of these three reports which form the basis of this paper.

† As a result of work subsequent to reference 2, Dr. Elata, in a private communication with the author, agreed that the mixing length constant does not appear to change and that a velocity profile shift does occur.

EFFECTS OF ELASTICITY ON THE UNIVERSAL VELOCITY PROFILE

The data in the paper of Ernst were obtained from the measured flow quantities and pressure drops in two pipe sizes (0.650 and 1.427 in. I.D.) as well as detailed velocity surveys across the pipes. The latter were presented in the form of the universal logarithmic velocity